

An artificial neural network methodology for damage detection: Demonstration on an operating wind turbine blade

Artur Movsessian^{a,*}, David García Cava^a, Dmitri Tcherniak^b

^a*School of Engineering, Institute for Infrastructure and Environment, University of Edinburgh, Alexander Graham Bell Building, Thomas Bayes Road, Edinburgh EH9 3FG, United Kingdom*
^b*Brüel & Kjær Sound and Vibration Measurements, Skodsborgvej 307, Nærum 2850, Denmark*

Abstract

This study presents a novel artificial neural network (ANN) based methodology within a vibration-based structural health monitoring framework for robust damage detection. The ANN-based methodology establishes the nonlinear relationships between selected damage sensitive features (DSF) influenced by environmental and operational variabilities (EOVs) and their corresponding novelty indices computed by the Mahalanobis distance (MD). The ANN regression model is trained and validated based on a reference state (i.e., a healthy structure). The trained model is used to predict the corresponding MD of new observations. The prediction error between the calculated and predicted MD is used as a new novelty index for damage detection. Firstly, an artificial 2D feature set is generated to illustrate how the limitations of solely using the MD-based novelty index can be overcome by the proposed ANN-based methodology. Secondly, the methodology is implemented in data obtained from an in-operation wind turbine with different artificially induced damage scenarios in one of its blades. Finally, the performance of the proposed methodology is evaluated by the metrics of accuracy, F1-score and Matthews correlation coefficient. The results demonstrate the advantages of the proposed methodology by improving damage detectability in all the different damage scenarios despite the influence of EOVs in both the simulated and real data.

Keywords: Artificial neural networks, damage detection, novelty index, Mahalanobis distance, environmental and operational variabilities

*Corresponding author

Email addresses: Artur.Movsessian@ed.ac.uk (Artur Movsessian), david.garcia@ed.ac.uk (David García Cava), dmitri.tcherniak@hbkwORLD.com (Dmitri Tcherniak)

1. Introduction

25 Wind is currently the second largest renewable energy source used for electricity generation [1]. The significant growth experienced by the wind energy industry and its rapidly falling costs per kilowatt-hour have made this sector highly competitive [2]. In order to succeed in such a competitive market, wind turbine (WT) developers have increased the diameter of the rotor to generate more energy with a single WT [3]. This has not only led to an increment in weight and size of the wind turbine blades (WTBs) but also to an
30 increment in their cost. Thus, monitoring the structural integrity of WTBs has become a relevant task for reliability and safety reasons.

Data-driven vibration-based structural health monitoring (VSHM) has been extensively studied in the past decades yet remains an active field of research. In the lowest level of VSHM, namely damage detection, researchers used to employ the Mahalanobis distance (MD) in order to identify discordant outliers in a data
35 set of observation which can be correlated to the presence of damage in the structure [4]. One of the prevailing challenges in MD-based damage detection is the presence of Environmental and Operational Variabilities (EOVs) impacting the accuracy of detecting damage. It was demonstrated in several studies [5–7] that the presence of EOVs can camouflage the presence of damage in a structure and ultimately reduce its detectability. Structures like WTs are generally exposed to severe influence from EOVs, especially when located offshore [8].
40 A study from Tcherniak et al. [9] evaluated operational vibration responses from a monitored Vestas V27 WT with several accelerometers mounted on one of the blades in order to detect artificially introduced damage. The study found a correlation between false alarms and temperature variations, thereby highlighting the influence of these variations on the accuracy of MD-based damage detection.

Researchers have sought to mitigate and filter EOVs to increase the damage detection accuracy. Considering that environmental and operational parameters are not always measured, output-only methods which exclusively use the measured vibration responses have been employed. The process of damage detection in an output-only VSHM system consists of the following main steps [10]: (i) Damage sensitive features (DSFs) extraction, i.e. features extracted from measured vibration responses that contain information about the structural integrity which allows to distinguish between a healthy and damaged structure, (ii) mitigating
45 EOVs to generate DSFs free from the influence of EOVs for robust novelty detection, (iii) novelty detection i.e. making an inference between observations from a healthy and a damaged structure. Selecting DSFs mostly depends on the structure in question. These can be physical quantities, e.g. natural frequencies and mode shapes which are commonly used [11–13], or DSFs that are considered more abstract such as statistical moments [14] and coefficients of parametric or non-parametric models [15–17]. Subsequently the DSFs
50 can be processed by linear or non-linear transformation tools e.g. Principal Component Analysis (PCA), Kernel PCA or Independent Component Analysis (ICA) are the most popular among many others. These transformations are used to compress and extract the most information regarding the structural integrity from the DSFs while reducing the effect of EOVs. Studies have shown that these transformations are capable of mitigating EOVs in DSFs whilst increasing the probability of successful damage detection [18–20]. More

60 recently, Cross et al. [21] adopted the concept of cointegration in order to identify statistical relationship between non-stationary variables. Researches have identified the advantages of the method and tested it in several studies generating fruitful results [21–24].

Other methods to mitigate the influence of EOFs consist of the use of machine learning algorithms. Particularly, the use of Artificial Neural Networks (ANNs) has gained popularity [25]. Despite the high
65 complexity and limited interpretability of ANNs, they can offer significant advantages, namely less formal statistical training is required due to their non-parametric nature or their ability to detect complex nonlinear relationships between independent and dependent variables [26]. ANNs served in several methodologies as a powerful tool for pattern recognition, specifically to learn the patterns of EOFs. For example, to reduce the false alarm rate in damage detection under varying temperature, Gu et al. [27] proposed a two-step procedure
70 where, first, auto-associative ANN is used to reconstruct modal parameters and, second, the novelty index was calculated by the Euclidean norm to highlight the reconstruction error. The methodology was tested on a finite element model and showed a high accuracy rate for different levels of noise. A study by Kostić et al. [28] employed ANNs for time-series analysis to mitigate the effects of temperature on the vibration response. The methodology was tested on a finite-element model of a footbridge where temperature effects
75 and damage scenarios were introduced. The results showed that the proposed methodology was able to determine the presence, location and, furthermore, the severity of the damage.

This paper contributes to the field of VSHM by proposing a novel methodology to mitigate the effects of EOFs in MD-based damage detection. For this, the DSFs extracted from vibration measurements of an operating wind turbine are labeled by the MD-metric which is influenced by the effects of EOFs as shown
80 by Tcherniak et al. [9]. A two-layer ANN regression model is built to learn how the presence of EOFs in DSFs affect the MD. Finally, the prediction error serves as a new novelty index. To highlight the novelty of the presented methodology, the limitations of the MD for novelty detection are presented. Further it is demonstrated how the combination of DSFs as predictors and the MD as a target are good candidates to use in a ANN regression model to mitigate EOFs. The proposed methodology is first implemented on simulated
85 two-dimensional data to demonstrate the procedure and merit of the method. To highlight the applicability on real structures, the methodology is tested on vibration responses obtained from the aforementioned operating Vestas V27 WT [9].

The paper is organized such that section 2 introduces the proposed methodology for damage detection and the metrics to evaluate its performance, followed by two case studies in section 3. Concluding remarks
90 are provided in section 4.

2. Methodology

The suggested ANN-based methodology is presented within a VSHM framework for statistical pattern recognition similar to the one described in [10]. The methodology is divided into the following four steps: (i) DSFs are extracted from the vibration responses collected when monitoring the dynamics of a structure. (ii) A subset of the collected DSFs is selected as a reference state and used to compute the Mahalanobis distance (MD) for the remaining DSFs. The MD serves as a label for the DSFs. (iii) An ANN regression model learns the relationships between the DSFs and their corresponding MD. This model is used to predict the MD for DSFs from new observations. (iv) A prediction error is computed and serves as the new novelty index for damage detection. The steps of the methodology are described more in detail in the following sections.

100 2.1. Damage sensitive feature for an output-only methodology

DSFs, which are application specific, are obtained from the measured vibration responses and stored in a DSF vector $\mathbf{f}^{(k)} \in \mathbb{R}^{q \times 1}$ which contains q DSFs for observation k . The DSF matrix $\mathbf{F} \in \mathbb{R}^{q \times r}$ is defined as follows:

$$\mathbf{F} = \begin{bmatrix} \mathbf{f}^{(1)} & \mathbf{f}^{(2)} & \dots & \mathbf{f}^{(k)} & \dots & \mathbf{f}^{(r)} \end{bmatrix} \quad (1)$$

where r is the number of observations. The split of the DSFs for training and testing the damage detection methodology is visualised in Fig. 1. The DSFs are split into training $\mathbf{F}_{hl,tr} \in \mathbb{F}^{q \times u}$ and testing $\mathbf{F}_{ts} \in \mathbb{F}^{q \times m}$,

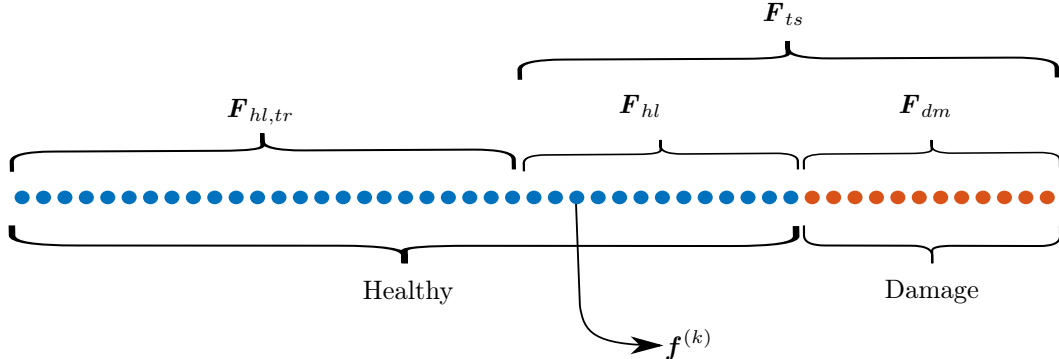


Figure 1: Data partitioning for an output-only damage detection methodology

105

where u is the number of training and m the number of testing observations. The testing set \mathbf{F}_{ts} contains a subset of healthy \mathbf{F}_{hl} and damaged \mathbf{F}_{dm} observations of the structure. For the output-only methodology, observations from the training set $\mathbf{F}_{hl,tr}$, that contain only healthy observations, are available to train the selected damage detection algorithm. The testing set \mathbf{F}_{ts} is used to assess the performance of the algorithm by identifying new healthy data \mathbf{F}_{hl} and further detecting damage in the structure with observations from \mathbf{F}_{dm} .

2.2. Mahalanobis distance

The MD measures the distance between a point and a distribution in an q-dimensional DSF space. As mentioned in the introduction, the MD is often used to identify outliers in a multivariate data set, whereas in this methodology, it serves as a label for the data for training the ANN. The MD is calculated as follows:

$$d^{(k)}(\mathbf{f}^{(k)}, \mathcal{F}) = \sqrt{(\mathbf{f}^{(k)} - \boldsymbol{\mu}_{\mathcal{F}})^T \boldsymbol{\Sigma}_{\mathcal{F}}^{-1} (\mathbf{f}^{(k)} - \boldsymbol{\mu}_{\mathcal{F}})} \quad (2)$$

where $d^{(k)}(\mathbf{f}^{(k)}, \mathcal{F})$ represents the MD between the feature vector $\mathbf{f}^{(k)}$ and the reference state created by the baseline matrix $\mathcal{F} \in \mathbf{F}^{q \times \hat{u}}$ with $\mathcal{F} \subset \mathbf{F}_{hl,tr}$ and $\hat{u} < u$, $\boldsymbol{\mu}_{\mathcal{F}}$ is the mean vector of the observations in \mathcal{F} and $\boldsymbol{\Sigma}_{\mathcal{F}}$ is the covariance between the observations in \mathcal{F} .

The Covariance matrix $\boldsymbol{\Sigma}_{\mathcal{F}}$ is positive semi-definite, therefore its inverse exists and is also positive semi-definite. The inverse can be presented by the Cholesky decomposition as follows: $\boldsymbol{\Sigma}_{\mathcal{F}}^{-1} = \mathbf{U}^T \mathbf{U}$, where \mathbf{U} is the upper triangular matrix, and the MD can be defined as follows [29]:

$$d^{(k)}(\mathbf{f}^{(k)}, \mathcal{F}) = \sqrt{(\mathbf{f}^{(k)} - \boldsymbol{\mu}_{\mathcal{F}})^T \mathbf{U}^T \mathbf{U} (\mathbf{f}^{(k)} - \boldsymbol{\mu}_{\mathcal{F}})}, \quad (3)$$

$$d^{(k)}(\mathbf{f}^{(k)}, \mathcal{F}) = \sqrt{(\mathbf{U}\mathbf{f}^{(k)} - \mathbf{U}\boldsymbol{\mu}_{\mathcal{F}})^T (\mathbf{U}\mathbf{f}^{(k)} - \mathbf{U}\boldsymbol{\mu}_{\mathcal{F}})}, \quad (4)$$

Thus, the MD is the Euclidean distance between the transformed DSFs space $\mathbf{U}\mathbf{f}^{(k)}$ and $\mathbf{U}\boldsymbol{\mu}_{\mathcal{F}}$.

2.3. Artificial neural networks

An ANN is a mathematical model widely used in the field of artificial intelligence due to its strong pattern recognition capability [30]. In this study, a two-layer feedforward ANN is adopted for the regression model to learn the existing patterns in DSFs which influence the MD-based novelty index. This structure has been used to approximate a nonlinear function in several studies [28, 31, 32]. The ANN structure is defined as:

$$g^{(k)}(\mathbf{f}^{(k)}, \mathbf{W}) = \sigma \left(\sum_{j=1}^N w_{kj}^{(2)} h \left(\sum_{i=1}^d w_{ji}^{(1)} f_i^k + w_{j0}^{(1)} \right) + w_{k0}^{(2)} \right), \quad (5)$$

where $g^{(k)}(\mathbf{f}^{(k)}, \mathbf{W}) \in \mathbb{R}^{u \times 1}$ is the set of estimated variables and $\mathbf{f}^{(k)} \in \mathbb{R}^{d \times 1}$ the DSFs for observation k . The output layer consists of the weights $w_{kj}^{(2)}$ and the bias $w_{k0}^{(2)}$, consequently $w_{ji}^{(1)}$ and $w_{j0}^{(1)}$ are the weights and the bias for the hidden layer. In the hidden layer, the hyperbolic tangent sigmoid activation function and a linear transfer function $\sigma(\cdot)$ for the output layer are implemented [33]. The least-square solution for training the weight matrix \mathbf{W} in Eq. 5 is obtained by minimizing E_D which is defined as follows:

$$E_D = \frac{1}{u} \sum_{k=1}^u [d^{(k)}(\mathbf{f}^{(k)}, \mathcal{F}) - g^{(k)}(\mathbf{f}^{(k)}, \mathbf{W})]^2, \quad (6)$$

where E_D is the mean-squared error between the prediction target $d^{(k)}(\mathbf{f}^{(k)}, \mathcal{F})$ and the ANN prediction $g^{(k)}(\mathbf{f}^{(k)}, \mathbf{W})$. To avoid a local minimum when minimizing Eq. 6, Bayesian regularization is introduced for supervised training. The cost-function E_D in Eq. 6 is extended to $S(\mathbf{W})$ as defined in MacKay [34]:

$$S(\mathbf{W}) = \beta \left(\frac{1}{u} \sum_{k=1}^u [d^{(k)}(\mathbf{f}^{(k)}, \mathcal{F}) - g^{(k)}(\mathbf{f}^{(k)}, \mathbf{W})]^2 \right) + \alpha E_{\mathbf{W}}, \quad (7)$$

where $E_{\mathbf{W}}$ is the mean-square sum of the weight matrix \mathbf{W} . In a Bayesian regularization framework, two objective functions α and β are added to penalize large weights. The ratio α/β between the objective functions is minimized leading the ANN function $g^{(k)}(\mathbf{f}^{(k)}, \mathbf{W})$ towards generalization (i.e. avoiding over- and under-fitting). The hyperparameters used in this study have been determined in a principled manner to build the ANN. The hyperparameters have been kept constant for both cases of study in order to demonstrate their capability to reproduce comprehensive and stable results. A brief summary of these parameters is presented in Appendix A.

140 2.4. ANN-based novelty index for damage detection

A regression model is built by training the ANN with the DSF vector $\mathbf{f}^{(k)}$ and the MD $d^{(k)}(\mathbf{f}^{(k)}, \mathcal{F})$ where $k : [1 < k \leq u]$. For the output-only methodology, the ANN function $g^{(k)}(\mathbf{f}^{(k)}, \mathbf{W})$ is trained exclusively with DSFs from a healthy structure $\mathbf{F}_{hl,tr}$ and their corresponding MD. The proposed novelty index for damage detection is obtained by the prediction error $\hat{d}^{(k)}$ between the predicted and calculated MD. This

145 ANN-based novelty index is defined as follows:

$$\hat{d}^{(k)} = \left| \log \frac{g^{(k)}(\mathbf{f}^{(k)}, \mathbf{W}) + \varepsilon}{d^{(k)}(\mathbf{f}^{(k)}, \mathcal{F}) + \varepsilon} \right| \quad (8)$$

where ε is a small scalar to avoid negative infinity due to DSFs that lay in the vicinity of the reference state, in this case $\varepsilon = 10^{-2}$. The ANN mapping function $g^{(k)}(\mathbf{f}^{(k)}, \mathbf{W})$ is trained with a unique relationship between the DSFs from the healthy structure and its target calculated by the MD metric. If an unlearned relationship between the features and the target occurs, due to e.g. damage in the structure, an increased prediction error is expected.

150 2.5. Evaluation of performance

Three classification metrics are used in this paper to evaluate the performance of the proposed methodology. The first is the *Accuracy* which is defined as:

$$Accuracy = \frac{TP + TN}{TP + TN + FP + FN}, \quad (9)$$

with *Accuracy* : $[0 \leq Accuracy \leq 1]$ where true positives (TP), false positives (FP), true negatives (TN) and false negatives (FN) represent a ratio of correctly predicted observations to the total number of observations. The accuracy measure is more appropriate for balanced data sets (i.e., equal number of healthy and damaged observations). Therefore, the F_1 -score metric is introduced as it is more suitable for unbalanced data sets. It is defined as follows [35]:

$$F_1 = \frac{2P_{pre} \times R_{rec}}{P_{pre} + R_{rec}} \quad (10)$$

with $F_1 : [0 \leq F_1 \leq 1]$ which is formed from the precision P_{pre} :

$$P_{pre} = \frac{TP}{TP + FP} \quad (11)$$

and the recall R_{rec} :

$$R_{rec} = \frac{TP}{TP + FN} \quad (12)$$

Despite the popularity of the accuracy and F_1 -score as performance measures used in many studies [36–38],

- 160** Matthews Correlation Coefficient (MCC) has been identified to provide more reliable and truthful scoring when evaluating binary classification as shown by Chicco and Giuseppe [39]. MCC is the third metric and is defined as:

$$MCC = \frac{(TP \times TN - FP \times FN)}{\sqrt{(TP + FP)(TP + FN)(TN + FP)(TN + FN)}}, \quad (13)$$

with $MCC : [-1 \leq MCC \leq 1]$. The maximum values for the three classification metrics are reached for perfect classification.

- 165** The cutoff value (or threshold) to pick the TP, FP and the corresponding TN and FN is the following [40–42]:

$$T(t) = \arg \min_t \sqrt{(1 - TP(t))^2 + (FP(t))^2}, \quad (14)$$

where t ranges over all possible thresholds. The threshold set, when $T(t)$ value is the minimum.

All three performance metrics are used for binary classification where the MD- and ANN-based damage detection are evaluated based on \mathbf{F}_{hl} as healthy and \mathbf{F}_{dm} as damaged.

170

3. Case Studies

In this section, two case studies are presented. The first case study consists of an artificially generated 2D feature set which are treated as DSFs highlighting the limitations of using the MD as a novelty index and the merit of the proposed methodology for robust damage detection. In the second case study, the applicability of the methodology is demonstrated on an operating Vestas V27 wind turbine for damage detection in a

- 175** WTB.

3.1. Artificial data set with 2D feature space

Artificial data is generated with 6000 observations, where $\mathbf{F} \in \mathbb{R}^{2 \times 6000}$ is the DSF matrix which is populated by $\mathbf{f}^{(k)} \in \mathbf{F}^{2 \times 1}$ DSFs for 6000 observations. As described in section 2.1, the data set is split into training data $\mathbf{F}_{hl,tr} \in \mathbf{F}^{2 \times 2000}$ and testing data $\mathbf{F}_{ts} \in \mathbf{F}^{2 \times 4000}$. The testing set \mathbf{F}_{ts} consists of $\mathbf{F}_{hl} \in \mathbf{F}_{ts}^{2 \times 2000}$ and $\mathbf{F}_{dm} \in \mathbf{F}_{ts}^{2 \times 2000}$. The partition of the data is summarised in Table 1.

Table 1: Partition of data for an output-only methodology: Simulated data set

	Healthy		Damage \mathbf{F}_{dm}	Total \mathbf{F}
	Training $\mathbf{F}_{hl,tr}$	Testing \mathbf{F}_{hl}		
Observations	2000	2000	2000	6000

To illustrate variabilities in the DSFs, the data from the healthy set is generated by a quadratic function with added Gaussian noise as shown in Fig. 2. Observations from the damaged state are within the distribution of the healthy class set but are clearly separated and do not overlap in the 2D feature space.

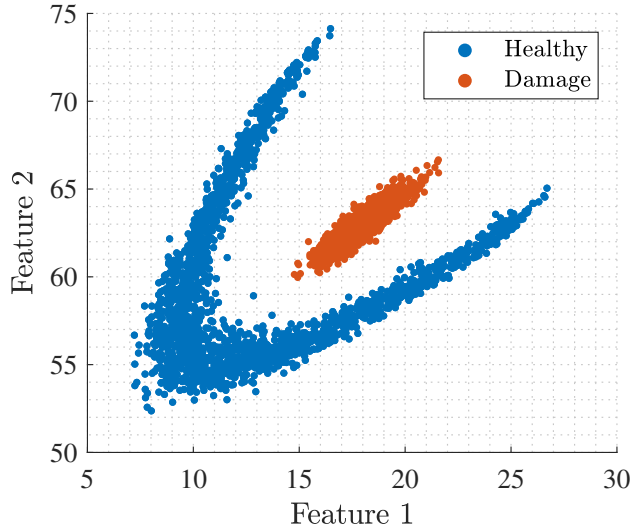


Figure 2: Artificial example - 2D plot of DSFs from a healthy state $\mathbf{F}_{hl,tr} \cup \mathbf{F}_{hl}$ and simulated damage DSFs \mathbf{F}_{dm}

3.1.1. Application of the Mahalanobis distance-based damage detection

To compute the MD-based novelty index presented in Eq. 2, the inverse covariance matrix $\mathcal{F} \in \mathbf{F}_{hl,tr}^{2 \times 2000}$ is decomposed and used to transform the DSFs by $\mathbf{U}\mathbf{f}^{(k)}$ and the reference $\mathbf{U}\boldsymbol{\mu}_{\mathcal{F}}$. The linear transformation of the DSFs is presented in Fig. 3a. The Euclidean distance is calculated from the normalised data set as per Eq. 5 resulting in the MD novelty index presented in a control chart in Fig. 3b.

It can be observed that the transformed DSFs in Fig. 3a have very little difference to the original DSF set in Fig. 2 as the introduced variabilities are still present. Due to the nonlinear relationship of the variables it is not sufficient to normalize the DSF set by the inverse covariance. The DSFs plotted in a 2D space show a clear separation between the healthy and damaged data sets. Nevertheless, once the Euclidean distance is calculated, the information regarding the location of the clusters is eliminated resulting in an overlapping novelty index. All data points on the threshold will have the same distance with different DSFs to the reference $\boldsymbol{\mu}_{\mathcal{F}}$ as shown in Fig. 3a. Discrimination between the two data sets is not possible due to the properties of the MD and the nature of this artificial set of DSFs with introduced variabilities.

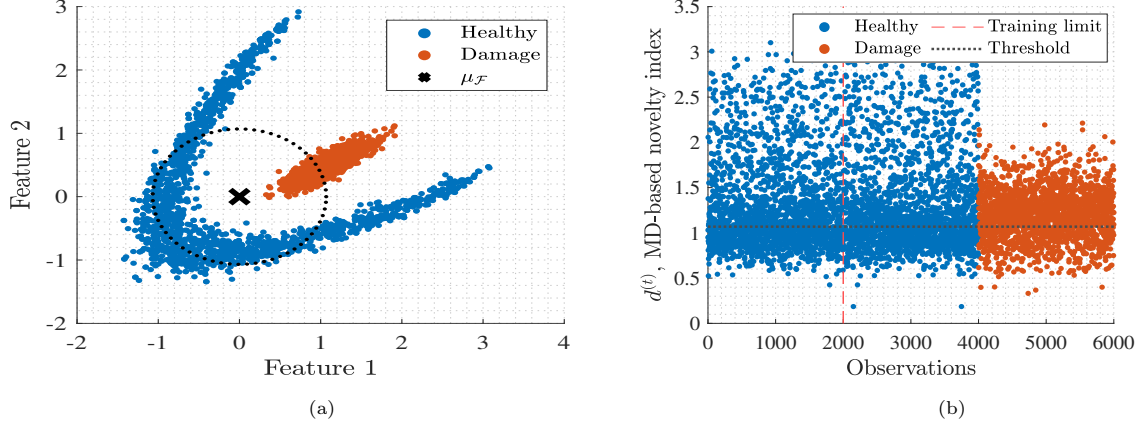


Figure 3: (a) Shows the transformed DSFs by $\mathbf{U}\mathbf{f}^{(k)}$ and $\mathbf{U}\boldsymbol{\mu}_{\mathcal{F}}$ where the dotted circle is the threshold calculated by Eq. 14. (b) MD-based novelty index obtained by the Euclidean distance after the transformation from figure (a)

3.1.2. Application of the ANN-based damage detection

Using the DSF set from section 3.1, the proposed damage detection methodology is applied to learn the relationship of the DSFs and their influence on the MD to overcome the limitation presented in section 3.1.1.

- 200 The complete data set is labeled by the MD presented in Eq. 2 with a reference matrix $\mathcal{F} \in \mathbf{F}_{hl,tr}^{q \times 200}$. The ANN regression function $g^{(k)}(\mathbf{f}^{(k)}, \mathbf{W})$ is trained with $\mathbf{F}_{hl,tr} \in \mathbf{F}^{2 \times 2000}$, with DSFs $\mathbf{f}^{(k)}$ and the MD label $d^{(k)}(\mathbf{f}^{(k)}, \mathcal{F})$ with $k : [1 \leq k \leq 2000]$. The calculated and predicted MD are presented in Fig. 4a. The novelty index calculated as per Eq. 8 is presented in a control chart in Fig. 4b. As only observations from the $\mathbf{F}_{hl,tr}$ are used to train the ANN, this results in an increment of the error if DSFs from the damaged set 205 are used to predict the MD as this relationship was not learned by the ANN regression model.

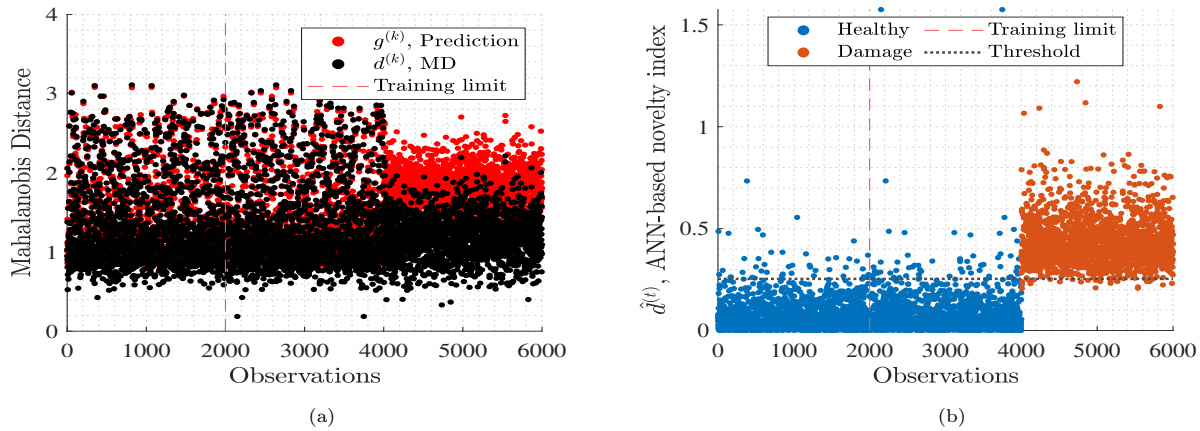


Figure 4: (a) Calculated MD $d^{(k)}(\mathbf{f}^{(k)}, \mathcal{F})$ and the predicted $g^{(k)}(\mathbf{f}^{(k)}, \mathbf{W})$ by ANN. (b) Prediction error $\hat{d}^{(k)}$ obtained by Eq. 8 for the artificial data set used as a new novelty index (ANN-based novelty index) for damage detection

The results from the performance metrics are presented in Table 2. The application of the suggested methodology was able to increase the accuracy of identifying novelties by predicting variabilities present in the MD-based novelty index and resulting in an improved separation of the two classes. The performance

- confirms the improvement in novelty detection with an increased accuracy and F_1 -score and MCC close to 1.
- 210 The information that was lost when calculating the MD is recovered by the ANN-based novelty index. For the MD-based novelty index, the accuracy and F_1 -score presented in Table 2 is 0.5377 and 0.5571 respectively. The MCC confirms these results with a value close to 0. These results show that detecting novelties is possible in around 50% of the cases.

Table 2: Classification results with \mathbf{F}_{hl} as healthy and \mathbf{F}_{dm} as damaged with artificial 2D DSFs

Performance metric	MD-based	ANN-based
Accuracy	0.5377	0.9870
F_1 -score	0.5571	0.9871
MCC	-0.0344	0.9741

3.2. Application on experimental data from an in-operation V27 wind turbine

- 215 To validate the proposed methodology in a realistic scenario, it was applied to the data obtained from the experiment conducted by Tcherniak et al. [9]. In the experiment, artificial damage was introduced on one of the WTBs of an operating Vestas V27 as shown in Fig. 5. The first introduced damage was a 15 cm trailing edge opening which was then extended to 30 cm, 45 cm and, finally, repaired. The WT, with a nominal power of 227 kW, has two main operational regimes: 32 and 43rpm. During the measurement campaign, the WT operated in both regimes. The experiment was conducted starting Nov. 28, 2014 and continued until March 12, 2015, i.e., the data collection campaign lasted almost 4 months.
- 220

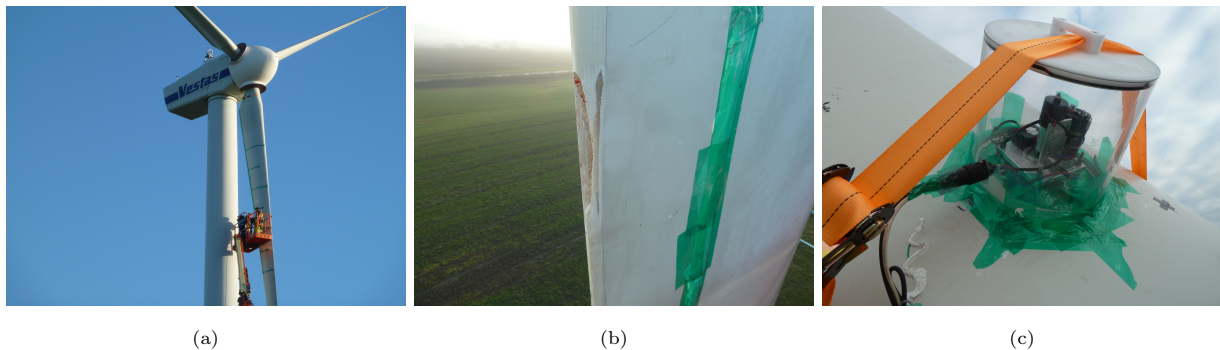


Figure 5: (a) Shows the Vestas V27 wind turbine. (b) First damage implemented by a 15cm trailing edge opening around 6m from the tip of the blade. (c) Electromagnetic actuator mounted close to the root of the blade for mechanical excitation.

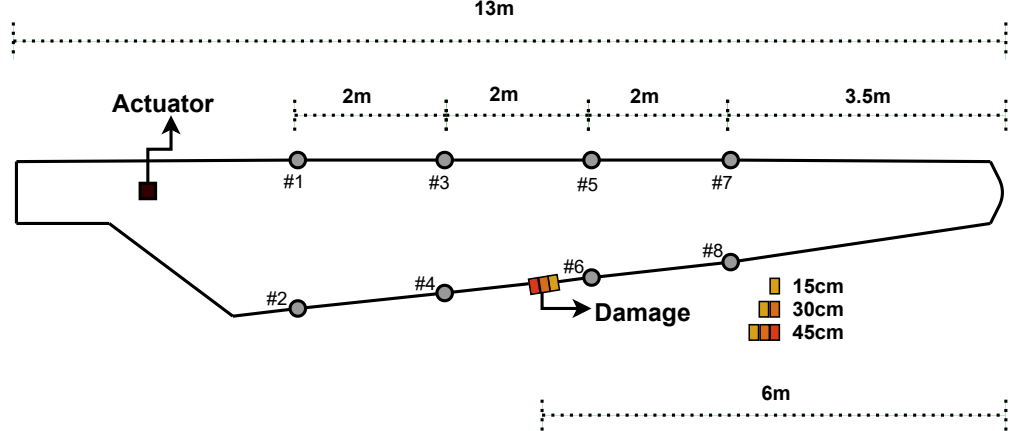


Figure 6: Sketch of the equipped WTB from the Vestas V27 based on [43]

The WTB has a total length of 13m and was equipped with 8 accelerometers (B&K accelerometers Type 4507 family) and an actuator installed at the root of the blade as shown in Fig. 6. The WTB was excited by the actuator and the vibration responses were captured by the 8 accelerometers with a sampling frequency of 225 16384 Hz. The data acquisition system started recording the responses 10 seconds before the actuator would hit the WTB and recorded for 20 seconds thereafter. Thus, the number of samples is approx. 500000 for the 30 seconds of recording corresponding to a hit from the actuator. For the duration of the experiment, a total number of 24693 actuator hits (observations) were recorded. A more detailed description of the experiment can be found in [9].

230 From the 24693 observations only the ones corresponding to 32 rpm operational regime were considered in this study. As the healthy state had a limited number of observations, 828, the repaired state with 2639 observations of the WTB is considered as healthy and as such is used as a reference to provide a sufficient amount of training data. The number of measurements are summarised in Table 3. Around 500000 data samples from each accelerometer recorded during an actuator hit were filtered by a band-pass filter with 235 cut-off frequencies of 700 and 1200 Hz. The filtered signal was trimmed and aligned to the 300 samples that corresponded to the highest amplitudes during the actuator hit [44].

As DSFs, the cross-covariance from each actuator hit between the accelerometer responses is calculated. The covariance is used as a measure of similarity between two signals, thus if a structural defect is acquired, the energy propagation from the actuator hit to the accelerometer will change its pattern. The cross-240 covariance matrix $\Sigma_{\mathcal{F}} \in \mathbb{R}^{a \times a}$ is symmetric, therefore unique values from the diagonal and upper triangle are obtained resulting in DSFs vectors with dimension $\frac{a(a+1)}{2}$, where a is the number of accelerometers used in the analysis. In this study, 4 accelerometers from the leading and 4 accelerometers from the trailing edge are considered resulting in a DSF vector $\mathbf{f}^{(k)} \in \mathbb{R}^{36 \times 1}$ with 36 unique covariance entries. The DSF matrix consists of 2927 observations with $\mathbf{F} \in \mathbb{R}^{36 \times 2927}$. The partition of the data for training and testing 245 is summarised in Table 3.

Table 3: Partition of data for an output-only methodology: Vestas V27 data set

	Healthy		Damage			Total \mathbf{F}
	Training $\mathbf{F}_{hl,tr}$	Testing \mathbf{F}_{hl}	\mathbf{F}_{dm15}	\mathbf{F}_{dm30}	\mathbf{F}_{dm45}	
Observations	2000	639	66	117	105	2927

The observations are split into training data $\mathbf{F}_{hl,tr} \in \mathbf{F}^{36 \times 2000}$ and testing data $\mathbf{F}_{ts} \in \mathbf{F}^{36 \times 927}$. The testing set contains a set of healthy data $\mathbf{F}_{hl} \in \mathbf{F}_{ts}^{36 \times 639}$ and three states of damage, namely 15cm damage $\mathbf{F}_{dm15} \in \mathbf{F}_{ts}^{36 \times 66}$, 30cm damage $\mathbf{F}_{dm30} \in \mathbf{F}_{ts}^{36 \times 117}$ and 45cm damage $\mathbf{F}_{dm45} \in \mathbf{F}_{ts}^{36 \times 105}$.

3.2.1. Application of the Mahalanobis distance-based damage detection for V27

First, the MD-based novelty index $d^{(k)}(\mathbf{f}^{(k)}, \mathcal{F})$ is calculated and presented in Fig. 7 with a reference set $\mathcal{F} \in \mathbf{F}_{hl,tr}^{36 \times 2000}$. Several deviations can be observed around observation 500, 1200 and more specifically at the end of the training after 2000 observations. Damage 1 with 15cm trailing edge opening is overlapping with \mathbf{F}_{hl} and some parts of the training data. Damage 2 with 30cm and damage 3 with 45cm trailing edge opening are well separated from the healthy data as well as from each other. The damage extension could be related to the increase of the MD.

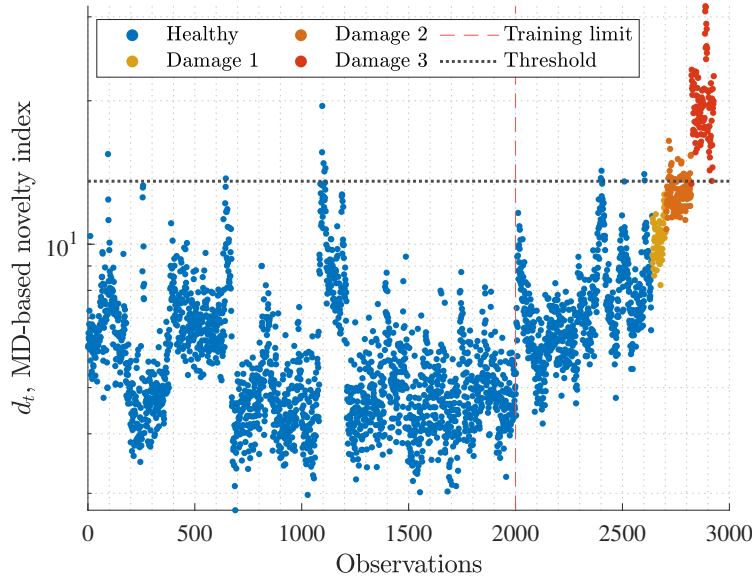


Figure 7: MD-based damage detection V27 calculated with healthy data (obtained from a repaired WTB) and three introduced damages

3.2.2. Application of the ANN-based damage detection for V27

The ANN-based novelty index is calculated in the same fashion as in section 3.2. The DSFs are labeled by the MD distance $d^{(k)}(\mathbf{f}^{(k)}, \mathcal{F})$ with $\mathcal{F} \in \mathbf{F}_{hl,tr}^{36 \times 200}$ which refers to the first 200 observations. The ANN

regression model is built with the DSFs $\mathbf{f}^{(k)}$ as predictors and their label (or learning target) $d^{(k)}$ where $k : [1 \leq k \leq 2000]$. Fig. 8a shows the calculated MD and the ANN prediction. The shift after 2000 observations is well-predicted by the proposed methodology as highlighted in Fig. 8b. Significant deviations in prediction occur after observation 2639 which corresponds to DSFs from a damaged WTB.

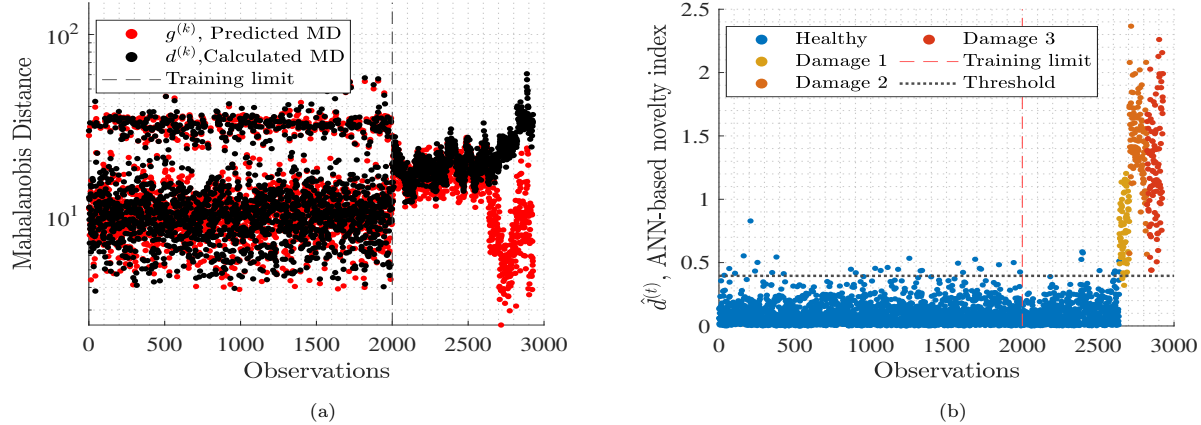


Figure 8: (a) Calculated MD $d^{(k)}(\mathbf{f}^{(k)}, \mathcal{F})$ and the predicted $g^{(k)}(\mathbf{f}^{(k)}, \mathbf{W})$ by ANN. (b) Prediction error $\hat{d}^{(k)}$ obtained by Eq. 8 for experimental data used as new novelty index (ANN-based novelty index) for damage detection

Table 4: Classification results with \mathbf{F}_{hl} as healthy and the three damage cases $\mathbf{F}_{dm15}, \mathbf{F}_{dm30}, \mathbf{F}_{dm45}$ for damage detection in V27 wind turbine

Performance metric	MD-based			ANN-based		
	Damage 1	Damage 2	Damage 3	Damage 1	Damage 2	Damage 3
Accuracy	0.861	0.967	0.993	0.986	0.997	0.995
F_1 -score	0.559	0.903	0.977	0.929	0.992	0.981
MCC	0.556	0.888	0.973	0.923	0.990	0.978

The overlap between the novelty indices from healthy and damaged states of the WTB was reduced, increasing the performance for all evaluation metrics as shown in Table 4. Significant improvement can be seen for the smallest damage with 15cm trailing edge opening which increased close to 1. This results from the high prediction accuracy for the test-set \mathbf{F}_{hl} where variabilities in the MD-based novelty index were well-predicted by the ANN. On the other hand, a bigger overlap in the different damage cases is observed, limiting the identification of damage propagation. For the MD-based novelty index, the accuracy decreases to 0.861, the F_1 -score to 0.559 and the MCC to 0.556 as presented in Table 4 for the smallest damage case.

270 4. Conclusions

EOVs in DSFs can camouflage the presence of damage, thereby reducing detectability. It is important to consider these variabilities and mitigate their effect on the novelty index. The work presented in this paper

proposed an ANN-based methodology within a vibration-based structural health monitoring framework for robust damage detection. The methodology consists of a two-layer ANN regression model aimed at learning
275 the relationships between DSFs and their corresponding novelty indices. The model was used to predict the MD-based novelty index in a continuous monitoring system where the presence of damage is highlighted through an increment in the prediction error. This prediction error represents the new ANN-based novelty index for damage detection.

The limitations of solely using the MD-based novelty index for damage detection were shown in an
280 artificial 2D DSF set, where accurate damage detection is hindered by variabilities in the DSFs. The proposed methodology sought to address these limitations and was tested on data collected from an operating Vestas V27 WT in order to detect different damage severities in one of its blades. The results show that all damage scenarios, introduced by a trailing edge opening from 15cm to 45cm, were detected despite the presence of EOVs. The number of false positives decreased whilst the number of true positives increased, resulting in
285 improved performance. The metrics of accuracy, F_1 -score and MCC increased in all cases resulting in higher reliability for damage detection.

Compared to the use of the MD-based novelty index, the proposed ANN-based methodology was not able to clearly distinguish between the different damage scenarios. However, a significant improvement can be observed when detecting the damage, especially for small ones which are more prone to be camouflaged
290 by the EOVs. Further research should be conducted to understand the nature of the relationships between DSFs, EOVs and the novelty index to better distinguish between different damage scenarios.

References

- [1] REN21, Renewables 2019 Global Status Report, Tech. rep., Paris: REN21 Secretariat (2019).
- [2] IRENA, Renewable Power Generation Costs in 2018, Tech. rep., International Renewable Energy Agency, Abu Dhabi (2019).
- [3] R. Wiser, M. Hand, J. Seel, B. Paulos, Reducing wind energy costs through increased turbine size: Is the sky the limit?, Lawrence Berkeley National Laboratory (2016).
- [4] K. Worden, G. Manson, N. R. Fieller, Damage detection using outlier analysis, *Journal of Sound and Vibration* 229 (3) (2000) 647–667.
- [5] H. Sohn, M. Dzwonczyk, E. G. Straser, K. H. Law, T. H.-Y. Meng, A. S. Kiremidjian, Adaptive modeling of environmental effects in modal parameters for damage detection in civil structures, in: Smart Structures and Materials 1998: Smart Systems for Bridges, Structures, and Highways, Vol. 3325, International Society for Optics and Photonics, 1998, pp. 127–138.
- [6] B. Peeters, J. Maeck, G. De Roeck, Vibration-based damage detection in civil engineering: excitation sources and temperature effects, *Smart materials and Structures* 10 (3) (2001) 518.
- [7] B. Peeters, G. De Roeck, One-year monitoring of the z24-bridge: environmental effects versus damage events, *Earthquake engineering & structural dynamics* 30 (2) (2001) 149–171.
- [8] C. Devriendt, F. Magalhães, W. Weijtjens, G. De Sitter, Á. Cunha, P. Guillaume, Structural health monitoring of offshore wind turbines using automated operational modal analysis, *Structural Health Monitoring* 13 (6) (2014) 644–659.
- [9] D. Tcherniak, L. L. Mølgaard, Active vibration-based shm system: demonstration on an operating vestas v27 wind turbine, in: 8th European Workshop On Structural Health Monitoring (EWSHM 2016), NDT.net, 2016, pp. 1–10.
- [10] C. R. Farrar, S. W. Doebling, D. A. Nix, Vibration-based structural damage identification, *Philosophical Transactions of the Royal Society of London. Series A: Mathematical, Physical and Engineering Sciences* 359 (1778) (2001) 131–149.
- [11] J. Kullaa, Damage detection of the z24 bridge using control charts, *Mechanical Systems and Signal Processing* 17 (1) (2003) 163–170.
- [12] N. Maia, J. Silva, E. Almas, R. Sampaio, Damage detection in structures: from mode shape to frequency response function methods, *Mechanical systems and signal processing* 17 (3) (2003) 489–498.
- [13] M. A. Wahab, Effect of modal curvatures on damage detection using model updating, *Mechanical Systems and Signal Processing* 15 (2) (2001) 439–445.

- [14] H. Martin, F. Honarvar, Application of statistical moments to bearing failure detection, *Applied acoustics* 44 (1) (1995) 67–77.
- ³²⁵ [15] L. D. Avendaño-Valencia, S. D. Fassois, Damage/fault diagnosis in an operating wind turbine under uncertainty via a vibration response gaussian mixture random coefficient model based framework, *Mechanical Systems and Signal Processing* 91 (2017) 326–353.
- [16] M. L. Fugate, H. Sohn, C. R. Farrar, Vibration-based damage detection using statistical process control, *Mechanical Systems and Signal Processing* 15 (4) (2001) 707–721.
- ³³⁰ [17] A. Behnia, H. K. Chai, A. A. Mousa, S. A. Ravanfar, A novel damage index for online monitoring of rc slabs under monotonic loading by integration of process controlling into acoustic emission technique, *Mechanical Systems and Signal Processing* 119 (2019) 547–560.
- [18] A.-M. Yan, G. Kerschen, P. De Boe, J.-C. Golinval, Structural damage diagnosis under varying environmental conditions—part i: a linear analysis, *Mechanical Systems and Signal Processing* 19 (4) (2005) 847–864.
- ³³⁵ [19] Y. Yang, S. Nagarajaiah, Blind identification of damage in time-varying systems using independent component analysis with wavelet transform, *mechanical systems and signal processing* 47 (1-2) (2014) 3–20.
- [20] Z. Yuqing, S. Bingtao, L. Fengping, S. Wenlei, Nc machine tools fault diagnosis based on kernel pca and-nearest neighbor using vibration signals, *Shock and Vibration* 2015 (2015).
- ³⁴⁰ [21] E. J. Cross, K. Worden, Q. Chen, Cointegration: a novel approach for the removal of environmental trends in structural health monitoring data, *Proceedings of the Royal Society A: Mathematical, Physical and Engineering Sciences* 467 (2133) (2011) 2712–2732.
- [22] B. A. Qadri, M. D. Ulriksen, L. Damkilde, D. Tcherniak, Cointegration for detecting structural blade damage in an operating wind turbine: An experimental study, in: *Dynamics of Civil Structures*, Volume 2, Springer, 2020, pp. 173–180.
- ³⁴⁵ [23] H. Shi, K. Worden, E. J. Cross, An exploratory study on removing environmental and operational effects using a regime-switching cointegration method, in: *Dynamics of Civil Structures*, Volume 2, Springer, 2017, pp. 329–337.
- [24] K. Worden, E. Cross, I. Antoniadou, A. Kyprianou, A multiresolution approach to cointegration for enhanced shm of structures under varying conditions—an exploratory study, *Mechanical Systems and Signal Processing* 47 (1-2) (2014) 243–262.
- ³⁵⁰ [25] Y. Lei, B. Yang, X. Jiang, F. Jia, N. Li, A. K. Nandi, Applications of machine learning to machine fault diagnosis: A review and roadmap, *Mechanical Systems and Signal Processing* 138 (2020) 106587.

- 355 [26] F. Ornelas-Tellez, J. J. Rico-Melgoza, A. E. Villafruerte, F. J. Zavala-Mendoza, Neural networks: A methodology for modeling and control design of dynamical systems, in: Artificial Neural Networks for Engineering Applications, Elsevier, 2019, pp. 21–38.
- [27] J. Gu, M. Gul, X. Wu, Damage detection under varying temperature using artificial neural networks, Structural Control and Health Monitoring 24 (11) (2017) e1998.
- 360 [28] B. Kostić, M. Güll, Vibration-based damage detection of bridges under varying temperature effects using time-series analysis and artificial neural networks, Journal of Bridge Engineering 22 (10) (2017) 04017065.
- [29] A. Bellet, A. Habrard, M. Sebban, Metric learning, Synthesis Lectures on Artificial Intelligence and Machine Learning 9 (1) (2015) 1–151.
- 365 [30] S. Samarasinghe, Neural networks for applied sciences and engineering: from fundamentals to complex pattern recognition, Crc Press, 2016.
- [31] J. Kudva, N. Munir, P. Tan, Damage detection in smart structures using neural networks and finite-element analyses, Smart Materials and Structures 1 (2) (1992) 108.
- 370 [32] D. Nguyen, B. Widrow, Improving the learning speed of 2-layer neural networks by choosing initial values of the adaptive weights, in: 1990 IJCNN International Joint Conference on Neural Networks, IEEE, 1990, pp. 21–26.
- [33] Y. LeCun, Y. Bengio, G. Hinton, Deep learning, nature 521 (7553) (2015) 436–444.
- [34] D. J. MacKay, Bayesian interpolation, Neural computation 4 (3) (1992) 415–447.
- 375 [35] G. Hripcsak, A. S. Rothschild, Agreement, the f-measure, and reliability in information retrieval, Journal of the American Medical Informatics Association 12 (3) (2005) 296–298.
- [36] P. Gardner, X. Liu, K. Worden, On the application of domain adaptation in structural health monitoring, Mechanical Systems and Signal Processing 138 (2020) 106550.
- 380 [37] C. Reich, A. Mansour, K. Van Laerhoven, Embedding intelligent features for vibration-based machine condition monitoring, in: 2018 26th European Signal Processing Conference (EUSIPCO), IEEE, 2018, pp. 371–375.
- [38] C. Sobie, C. Freitas, M. Nicolai, Simulation-driven machine learning: Bearing fault classification, Mechanical Systems and Signal Processing 99 (2018) 403–419.
- [39] D. Chicco, G. Jurman, The advantages of the matthews correlation coefficient (mcc) over f1 score and accuracy in binary classification evaluation, BMC genomics 21 (1) (2020) 6.

- ³⁸⁵ [40] R. Kumar, A. Indrayan, Receiver operating characteristic (roc) curve for medical researchers, *Indian pediatrics* 48 (4) (2011) 277–287.
- [41] A. K. Akobeng, Understanding diagnostic tests 3: receiver operating characteristic curves, *Acta paediatrica* 96 (5) (2007) 644–647.
- ³⁹⁰ [42] Y.-T. Hwang, Y.-H. Hung, C. C. Wang, H.-J. Terng, Finding the optimal threshold of a parametric roc curve under a continuous diagnostic measurement, *REVSTAT–Statistical Journal* 16 (1) (2018) 23–43.
- [43] M. D. Ulriksen, D. Tcherniak, L. Damkilde, Damage detection in an operating vestas v27 wind turbine blade by use of outlier analysis, in: 2015 IEEE Workshop on Environmental, Energy, and Structural Monitoring Systems (EESMS) Proceedings, IEEE, 2015, pp. 50–55.
- ³⁹⁵ [44] D. Tcherniak, L. L. Mølgaard, Active vibration-based structural health monitoring system for wind turbine blade: Demonstration on an operating vestas v27 wind turbine, *Structural Health Monitoring* 16 (5) (2017) 536–550.

Appendix A. Artificial Neural Networks and Hyperparameters

The structure of the ANN shown in Table A.5 consists of q input nodes, which refers to the amount of damage sensitive features. $q = 2$ for the artificial data set and $q = 36$ for the experimental data from an in-operation V27 wind turbine.

Table A.5: Artificial neural network architecture and activation functions

Network Architecture	Hidden Layer Activation Function	Output Layer Activation Function
q-2-1	Hyperbolic Tangent Sigmoid Activation Function	linear transfer function

A total number of 2000 iterations is set for learning and generalizing the weights in the Bayesian back-propagation. The learning rate is set to 0.005. The training stops when the optimal combination of errors and weights is found that minimized the mean squared error. The same hyperparameters are used in both case studies for training and validation of the model.